ACS APPLIED MATERIALS & INTERFACES

Research Article

www.acsami.org

# Shieldable Tumor Targeting Based on pH Responsive Self-Assembly/Disassembly of Gold Nanoparticles

Zhiqing Tian, Chengling Yang, Wei Wang, and Zhi Yuan*

Key Laboratory of Functional Polymer Materials of Ministry of Education and Institute of Polymer Chemistry, Nankai University Collaborative Innovation Center of Chemical Science and Engineering, Tianjin 300071, China

Supporting Information

**ABSTRACT:** A new approach to shield/deshield ligands for controllable tumor targeting was reported, which was based on amphiphilic self-assembly and disassembly of gold nanoparticles (Au NPs). Thanks to the excellent pH response of the system, glycyrrhetinic acid (GA) ligands can be buried inside the Au NPs' assembly at normal tissue pH (pH 7.4), while exposed when the nanostructure is disassembled at tumor extracellular pH (pHe 6.8). Hydrophobic GA molecules not only acted as ligands targeting tumor cells but also provided the major interparticle attractive force for Au NPs' assembling. An ordered assembly of Au NPs with regular shape, proper size and ultrasharp pH sensitivity (ΔpH ∼ 0.2) was achieved by fine-tuning of materials modified on Au NPs. Mechanism studies for assembly and disassembly of Au NPs indicated the possibility of a GA shield when the assembly formed, which was further demonstrated by bovine serum albumin absorption and cellular uptake. The assembly/disassembly process was reversible within extrinsic pH changes, which provides a perspective for reversible tumor targeting.

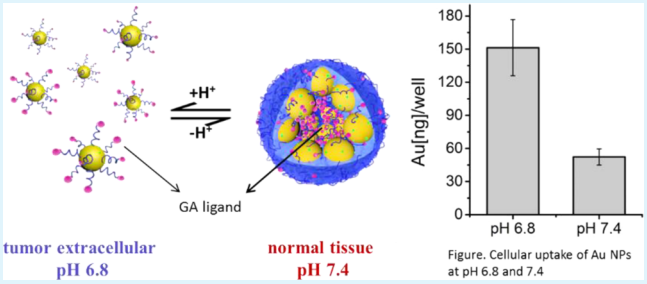

Figure. Cellular uptake of Au NPs at pH 6.8 and 7.4

**KEYWORDS:** *tumor targeting, self-assembly, gold nanoparticle, pH-responsive, drug delivery*

## 1. INTRODUCTION

Drug delivery systems based on nanoparticles hold enormous potential in cancer therapy for their improved pharmacokinetics and minimal nonspecific toxicity.[1−3] Despite experimental and clinical success, drug delivery still faces challenges including prolonging the delivery half-time and achieving high accumulation with high selectivity at the tumor site. These challenges arise from the complexity of several hurdles during delivery, such as reticuloendothelial system (RES) clearance, target accumulation and cellular internalization.[4] Contradictory attributes of nanoparticles are often required to overcome these hurdles.[5,6] For instance, surface functionalization with biologically active ligands facilitates the targeting of specific cells, but may lead to immune recognition or undesirable cellular uptake in the bloodstream and normal tissue.[7,8] To address this challenge, strategies have been developed where the ligand display of nanocarriers can be tuned, stimulated by changes in the microenvironment, so that the targeting ability of NPs is shielded during delivery but activates once they have arrived at the tumor site. The slight difference of pH existing between blood (∼7.4) and the extracellular environment of solid tumors (6.5−7.2) is often utilized as the stimulation.[9] Frequent approaches to harness the targeting activity typically depend on surface alteration of nanocarriers, such as detaching stealth coatings, "popping up" ligands and removing inhibitors.[9−16]

On the other hand, approaches based on the stimuli-responsive assembly of amphiphilic materials efficiently modulate the interfacial density of ligands, which provides a new method to tune the cellular uptake.[17−19] Due to the reversible property for amphiphilic self-assembly and disassembly, these approaches show potential to surmount the irreversibility of traditional targeting shielding, which causes off-target accumulation or RES clearance if the deshielded carrier leaks out of the tumor.[18] Chilkoti and his co-workers reported that the cellular uptake of drug carrier was amplified by self-assembly of a genetically encoded polypeptide with an enhanced ligand density.[17] However, thus far, activating targeting ability by the disassembly of nanostructures has rarely been investigated. The pH-sensitive fabrication assembled from amphiphilic NPs (e.g., inorganic amphiphilic NPs) provides a unique opportunity to hide hydrophobic ligands into the assembly at pH 7.4, whereas the disruption of the assembly at pH 6.8 enables ligands' exposure for tumor targeting. Importantly, the assembly with a proper size (100−200 nm) in the blood facilitates an enhanced permeation and retention (EPR) effect to achieve high target accumulation, whereas the disassembled particles with smaller sizes at tumors penetrate tumors more rapidly and uniformly than larger particles.[20,21]

For this purpose, a nanostructure with sharp pH sensitivity is desirable to respond to the subtle pH differences between solid tumors and the normal tissue environment. Recently, stimuli-responsive materials have been utilized in nanostructures

Received: July 11, 2014
Accepted: September 18, 2014
Published: September 18, 2014

   dx.doi.org/10.1021/am5045339 | ACS Appl. Mater. Interfaces 2014, 6, 17865−17876

**Scheme 1. Schematic Illustration of GA Ligand's Shield at Blood pH (pH 7.4) and Exposure at Tumor Extracellular Environment pH (pH 6.8), and Possible Mechanism of Sharp pH-Responsive Assembly and Disassembly of Au NPs**

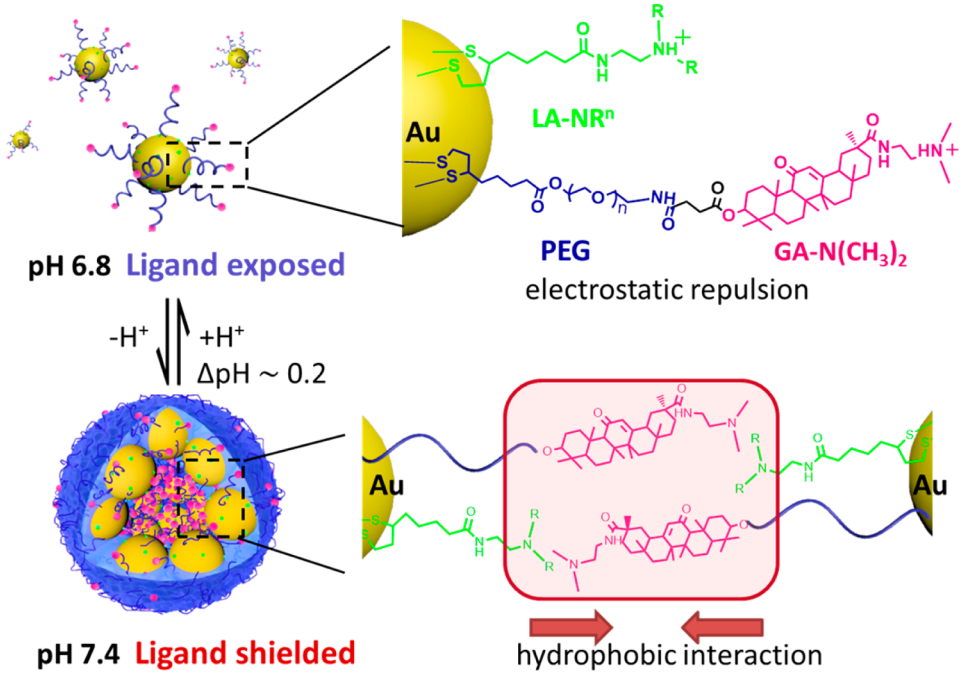


fabricated by gold nanoparticles (Au NPs) for pH-induced disassembly, which have been exploited in areas such as tumor sensing and treatment.[22−26] However, their pH response is not sharp enough to meet our requirement.

Herein, we demonstrate an approach to shield and deshield ligands for controllable tumor targeting by the amphiphilic self-assembly and disassembly of gold nanoparticles. To achieve this goal, we developed a rapid and green method to assemble Au NPs, which enabled Au NPs assembly or disassembly with ultrasensitive pH response (ΔpH ~ 0.2). Lipoyl tertiary amines (further denoted as LA-NR$^n$), together with a unique well-designed poly(ethylene glycol) (PEG) (PEG-GA-N$(CH_3)_2$), were introduced to the model (Scheme 1). Glycyrrhetinic acid (GA) is a targeting ligand that shows distinguished targeting efficiency to hepatocytes.[27,28] Importantly, it was also used as the hydrophobic segment immobilized on the PEG terminal to tune the hydrophilicity of PEG and act as the major source of hydrophobic force for interparticle attraction. Amphiphilicity-driven self-assembly enables the shielding of hydrophobic GA ligands inside, into the hydrophobic core of the assembly. The assembly dispersed into single Au nanoparticles immediately in a more acidic environment (e.g., pH 6.8) that was promoted by a protonated and positively charged amino group (ΔpH ~ 0.2). This endowed the nanocarriers with exposure of the GA ligands, facilitating cellular uptake of Au NPs.

## 2. MATERIALS AND METHODS

**2.1. Materials.** Glycyrrhetinic acid (GA, HPLC purity >98%) was purchased from Fujie Pharmaceutical Co., Ltd. (Xi'an, China). *N*,*N*-dimethylethylenediamine (DMEDA), *N*-hydroxysuccinimide (NHS), *N*,*N*′-dicyclohexylcarbodimide (DCC), *N*-(3-(dimethylamino)propyl)-*N*′-ethylcarbodiimide hydrochloride (EDC·HCl), succinic anhydride, 4-dimethylamiopyridine (DMAP) and 1-hydroxybenzotriazole (HOBt) were obtained from Aladdin Industrial Co. (Shanghai, China). $NH_2$-$PEG_{3.4k}$-OH and m$PEG_{2k}$-$NH_2$ were purchased from Seebio Biotech, Inc. (Shanghai, China). α-Lipoic acid (LA), 1-(2-aminoethyl)pyrrolidine and 2-aminoethyldiisopropylamine were purchased from Adamas Reagent Co. (Shanghai, China). *N*-(2-Aminoethyl)piperidine and Nile red were purchased from J&K Scientific Ltd. (Beijing, China). *N*,*N*-Dibutylethylenediamine, trisodium citrate dehydrate and pyrene were purchased from Alfa Aesar Company. Chloroauric acid was purchased from Acros Company. A BCA kit was purchased from Beyotime Institute of Biotechnology (Jiangsu, China). Citric acid-stabilized AuNPs (~26 nm, measured by DLS) were prepared according to the literature.[29] The water used was prepared using Millipore Elix System (Millipore, Bedford, MA). Other solvents were used as received without further purification.

**2.2. Measurements.** $^1$H NMR spectra were collected on a Bruker 400 MHz spectrometer. Tetramethylsilane (TMS) was used as the internal reference. High resolution electrospray ionization mass spectrometry (HRESI-MS) and infrared (IR) were performed on Agilent 6520 and Bio-Rad FTS 6000 instruments, respectively. Matrix-assisted laser desorption/ionization time-of-flight (MALDI-TOF) MS spectra were collected on Bruker AutoflexIII LRF200-CID. Dynamic light scattering (DLS) experiments were performed with a Zetasizer Nano-ZS90 instrument (Malvern Instruments Ltd., UK) at room temperature. To measure size of Au NPs at different pH, the solution of preassembled nanoparticles was diluted using 50 mM 4-(2-hydroxyethyl)-1-piperazineethanesulfonic acid (HEPES) with pH varying from 6.6 to 8.2. The morphology and size of Au NPs were examined on a Tecnai G2 F20 transmission electron microscope (FEI, USA). UV spectra were obtained on SHIMADZU UV-2550 (Japan). The fluorescence emission spectra were obtained on a Hitachi fluorometer (F-7000, Hitachi, Japan).

**2.3. Synthesis of GA Derivatives (Scheme 2).** Compound **2** was generally prepared by the literature procedures.[30] DCC (2.60 g, 12 mmol) and HOBt (2.00 g, 12 mmol) were dissolved in dichloromethane (DCM) (30 mL) and stirred at RT for 30 min. Glycyrrhetinic acid **1** (4.80 g, 10.0 mmol) was added to this solution, and the mixture was stirred for 20 min. DMEDA (1.1 mL, 6 mmol) was added, and the mixture was stirred at RT for 12 h. The solvent was evaporated in vacuo and the residue purified by chromatography (dichloromethane (DCM)/MeOH/$NH_3$·$H_2O$ elution, 15:1:1). Then the residue was resolved in EtOAc and filtered, and the solvent evaporated in vacuo and obtained product **2** as a white powder (5.10 g, 94% yield). $^1$H NMR (Bruker 400 MHz, $CDCl_3$, TMS): $\delta$ = 6.63 (m, 1H), 5.89 (s, 1H), 3.43 (m, 1H), 3.27 (m, 1H), 3.22 (m, 1H), 2.76 (m, 1H),

**Scheme 2. Synthesis of GA Derivatives and LA-PEG-GA-N$(CH_3)_2$**

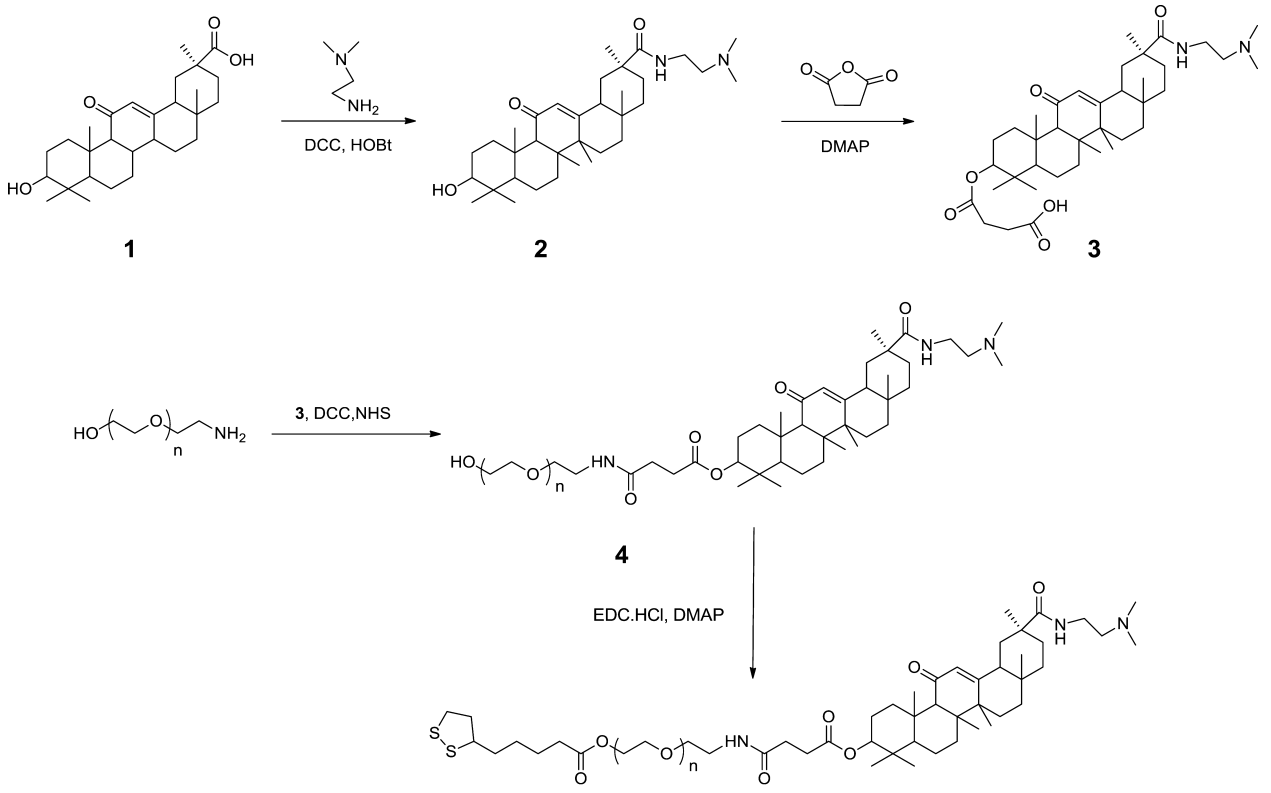


2.28 (s, 6H), 2.11−1.51 (m, 26H), 1.10 (s, 9H), 1.00 (s, 3H), 0.76 (s, 3H), 0.73 (s, 3H). HRESI-MS: 541.4373 (M + 1).

To the solution of compound **2** (3.20 g, 5.8 mmol) in dry pyridine was added succinic anhydride (4.70 g, 47 mmol) and DMAP (7.70 g, 58 mmol). The mixture was heated at 90 °C for 8 h. After pyridine was removed by evaporation in vacuo, the residue was eluted using chromatography with mobile phase (DCM/MeOH/$NH_3{\cdot}H_2O$ = 15/1/1, then turned to $CH_2Cl_2$/MeOH = 15/1) to obtain the brown product **3** (2.4 g, 65% yield). $^1$H NMR (400 MHz, $CDCl_3$): $\delta$ = 5.57 (s, 1H), 4.47 (m, 1H,) 3.76 (s, 1H), 3.51 (m, 1H), 3.03 (m, 1H), 2.54 (s, 6H), 2.25−1.55 (m, 27H), 1.45 (s, 3H), 1.15 (s, 3H), 1.14 (s, 3H), 1.10 (s, 3H), 0.85 (s, 6H), 0.8 (s, 3H). HRESI-MS: 641.4533 (M + 1).

**2.4. Synthesis of LA-PEG-GA-N$(CH_3)_2$ (Scheme 2).** Compound **3** (320 mg, 0.5 mmol), DCC (103 mg, 0.5 mmol) and NHS (57 mg, 0.5 mmol) were stirred in DCM at 0 °C. $NH_2$-$PEG_{3.4k}$-OH (1700 mg, 0.5 mmol) was added to this mixture, and the mixture was stirred for 30 min at 0 °C, then heated to 35 °C for 2 d. The solution was filtered to remove the precipitate, followed by precipitation in cold diethyl ether and vacuum drying overnight to obtain **4**. Then $\alpha$-lipoic acid (515 mg, 2.5 mmol), EDC·HCl (479 mg, 2.5 mmol) and DMAP (305 mg, 2.5 mmol) were added to the DCM solution of **4**, and the mixture was stirred at 0 °C for 20 min. The flask was then heated to 60 °C for 2 d. After reaction, the solution was filtered to remove the precipitate, and the DCM solvent was removed by rotovap. The resulting residue was resolved in water, and the insoluble residue was removed by centrifugation. The product was dialyzed against water at RT for 2 d within a dialysis tubing (MWCO 3500, Spectrum, US) and was obtained after lyophilization as a white powder. Compound **5** was characterized by $^1$H NMR and MALDI-TOF MS, which is shown in Figures 1 and 2.

**2.5. Synthesis of mPEG-GA-N$(CH_3)_2$.** To a solution of **3** (320 mg, 0.5 mmol) and $mPEG_{2k}$-$NH_2$ (1000 mg, 0.5 mmol) in dry THF (10 mL) at 0 °C was added NHS (70 mg, 0.6 mmol) and DCC (125 mg, 0.6 mmol), and the mixture was stirred at 0 °C for 30 min. Then the mixture was heated to reflux for 24 h. After the solution cooled to RT, the reaction mixture was filtered, and THF was evaporated in vacuo to get a white residue. It was purified by chromatography ($CH_2Cl_2$:MeOH:$NH_3{\cdot}H_2O$ = 15:1:1) to get a white-like powder (1240 mg, 94.5% yield).

**2.6. Synthesis of LA-NR$^n$ Derivatives.** LA-NR$^n$ derivatives were synthesized following a similar method (Scheme 3). Synthesis of LA-N$(iPr)_2$ (LA-NR$^4$) is described as a representative procedure. Lipoic acid (206 mg, 1.0 mmol) and 2-aminoethyldiisopropylamine (144 mg, 1.0 mmol) were stirred in DCM at RT for 30 min. EDC·HCl was added to the mixture and stirred at 35 °C for 6 h. After reaction, the solution was washed with water, dried with $Na_2SO_4$ and the solvent was removed in vacuo to obtain LA-N$(iPr)_2$ as a yellow solid. The products were characterized by $^1$H NMR, HRESI-MS and IR.

LA-NR$^1$ $^1$H NMR ($CDCl_3$): $\delta$ = 3.57 (m, 1H), 3.34 (m, 2H), 3.15 (m, 2H), 2.44 (m, 3H), 2.27−2.14 (m, 8H), 1.90 (m, 1H), 1.66 (m, 4H), 1.44 (m, 2H). ESI-MS: 277.1409 (M + 1). IR: $\nu$ ($cm^{-1}$) = 3297, 3071, 2933, 2817, 2768, 1645, 1544, 1459, 1356, 1251.

LA-NR$^2$ $^1$H NMR ($CDCl_3$): $\delta$ = 3.54 (m, 1H), 3.32 (m, 2H), 3.12 (m, 2H), 2.56−2.48 (m, 7H), 2.17 (m, 2H), 1.89 (m, 1H), 1.75 (m, 4H), 1.65 (m, 4H), 1.46 (m, 2H). ESI-MS: 303.1569 (M + 1). IR: $\nu$ ($cm^{-1}$) = 3294, 3070, 2931, 2787, 1649, 1541, 1457, 1351, 1290, 1254.

LA-NR$^3$ $^1$H NMR ($CDCl_3$): $\delta$ = 3.55 (m, 1H), 3.30 (m, 2H), 3.12 (m, 2H), 2.45−2.30 (m, 7H), 2.19 (m, 2H), 1.90 (m, 1H), 1.70−1.65 (m, 8H), 1.55−1.40 (m, 4H). ESI-MS: 317.1726 (M + 1). IR: $\nu$ ($cm^{-1}$) = 3296, 3075, 2933, 2852, 1648, 1441, 1351, 1255.

LA-NR$^4$ $^1$H NMR ($CDCl_3$): $\delta$ = 3.55 (m, 1H), 3.23 (m, 2H), 3.11 (m, 2H), 3.04 (m, 2H), 2.60 (m, 2H), 2.43 (m, 1H), 2.20 (m, 2H), 1.95 (m, 1H), 1.65 (m, 4H), 1.44 (m, 2H), 1.03 (d, 12H). ESI-HRMS: 333.2030 (M + 1). IR: $\nu$ ($cm^{-1}$) = 3297, 3076, 2931, 2864, 1660, 1360, 1254.

LA-NR$^5$ $^1$H NMR ($CDCl_3$): $\delta$ = 3.55 (m, 1H), 3.28 (m, 2H), 3.18 (m, 2H), 2.53 (m, 2H), 2.42 (m, 5H), 2.20 (m, 2H), 1.93 (m, 1H), 1.66 (m, 4H), 1.48−1.40 (m, 6H), 1.31 (m, 4H), 0.92 (m, 6H). ESI-HRMS: 361.2345 (M + 1). IR: $\nu$ ($cm^{-1}$) = 3295, 3076, 2953, 2800, 1645, 1545, 1459, 1392, 1375, 1254.

**2.7. Surface Modification and Self-Assembly of AuNPs.** Excess LA-NR$^n$ (4 mg) and LA-PEG-GA-N$(CH_3)_2$ (4 mg) were stirred in 3 mL

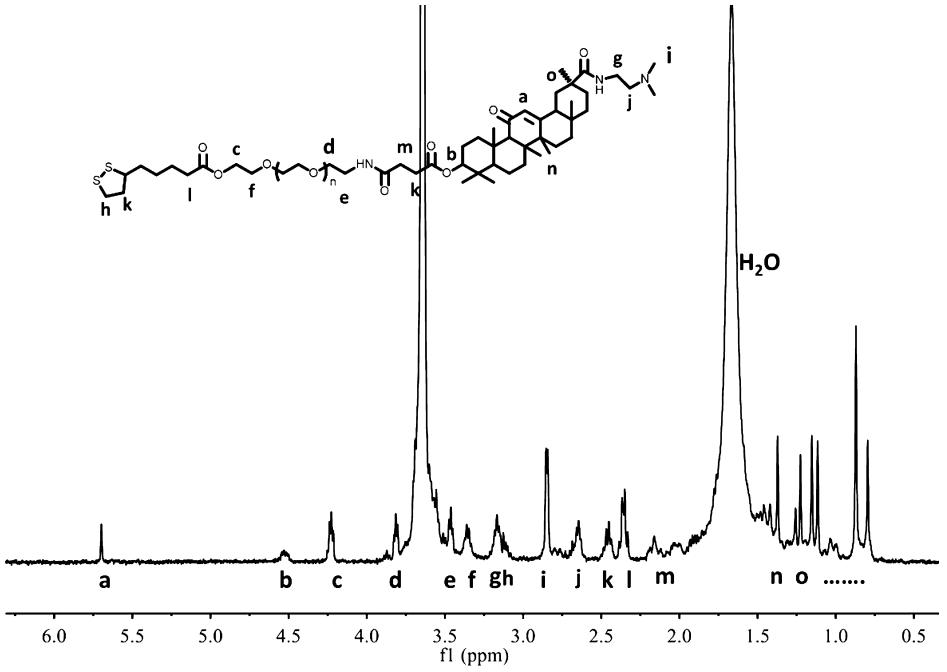


**Figure 1.** 400 MHz $^1$H NMR spectra of LA-PEG-GA-N$(CH_3)_2$ in $CDCl_3$.

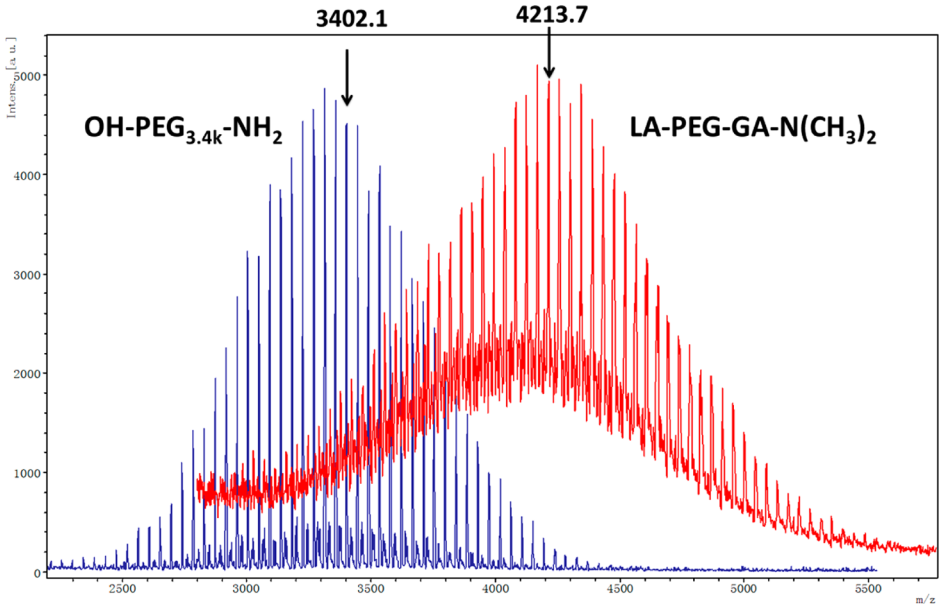


**Figure 2.** MALDI-TOF MS spectra of LA-PEG-GA-N$(CH_3)_2$ (red) and its starting OH-PEG-$NH_2$ (blue).

of $H_2O$ for 20 min at pH 4. Then 9 mL of gold nanoparticle dispersion (10 nM) was added to the mixture and the resulting solution was stirred at RT for 6 h. The molar ratio (LA-PEG-GA-N$(CH_3)_2$:LA-NR$^n$) of the two grafts carried by Au NPs, on average, as calculated from $^1$H NMR according to the method in literature,[22] is about 1.7:1. The signal of the methylene protons of PEG block on PEG-GA-N$(CH_3)_2$ and methyl protons of iPr on LA-NR$^4$ were used as characteristic peaks to calculate the molar ratio of these two grafts.

The self-assembly of AuNPs is based on simple high-speed shake. Briefly, the resulting solution was allotted 0.4 mL into each plastic tube, diluted 1:1 with milli-Q water and adjusted pH to ~9 using NaOH. The mixed solution was shook using a vortexer for 1−2 min with high speed, and then stood for 1 d. After the formation of the assembly, the solution was dialyzed against dilute NaOH solution (pH 8−9) for 48 h (MWCO 8000−15 000, Spectrum, USA) to remove unconjugated polymers and amine molecules.

**2.8. Investigating the Improvement of Hydrophilicity of GA-N$(CH_3)_2$ Using mPEG-GA$(CH_3)_2$.** The improvement of GA-N$(CH_3)_2$ was demonstrated through investigating the size of nanoparticle formed by mPEG-GA$(CH_3)_2$, whose size is pH-dependent. mPEG-GA$(CH_3)_2$ (7 mg) was first dissolved in 1 mL of acetone and then added into 4 mL of stirring aqueous solution (4 mL) (pH 3−9) dropwise. The acetone was allowed to evaporate for 1 h by air stream. The nanoparticles were characterized by DLS for hydrodynamic diameter.

**2.9. Fluorescence Characterization.** The fluorescence probes were loaded into NPs easily by a film-rehydration method.[22] Preparation of the pyrene loaded assembly was described as a representative procedure. First, a AuNPs (dispersed) aqueous solution was lyophilized to obtain solid AuNPs. Then 300 $\mu$L of DCM solution and 3 $\mu$g of pyrene were codeposited with the gold nanoparticle (3 mg) into 3 mL of DCM. The solution was thoroughly dried in vacuo to form a film on the wall of a glass vial, and then 2 mL of pH 9 NaOH solution was added to

**Scheme 3. Synthesis of LA-NR$^n$ Derivatives**

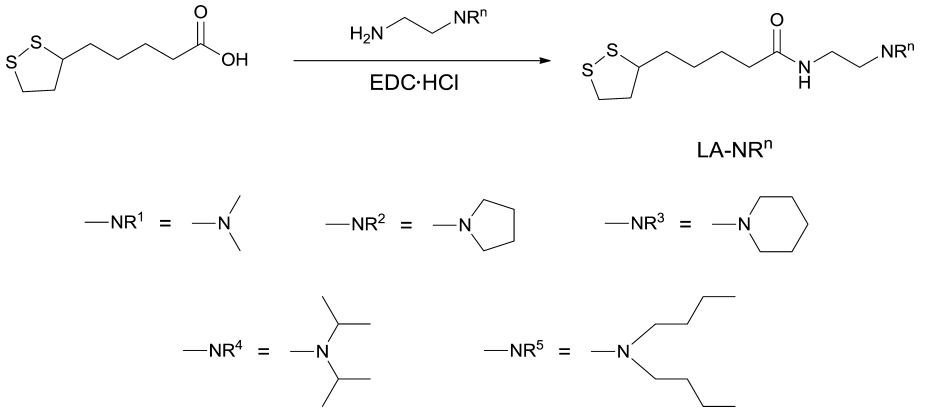


rehydrate the film under sonication. The fluorescence was examined after left standing for 12 h.

The stock solution was was diluted in 50 mM HEPES buffers with different pH values (1:4). The nanoprobe for pyrene was excited at 334 nm, and the emission spectra were collected from 350 to 500 nm. Nile red, as the fluorescent probe, was excited at 540 nm, and the range of emission spectra was from 560 to 650 nm.

**2.10. Bicinchoninic acid (BCA) Assay.** Samples (assemble and dispersed) were immersed in bovine serum albumin (BSA) solution (0.48 g $L^{-1}$, prepared in HEPES buffer, pH 7.4 and 6.8), respectively, followed by an incubation at RT for 1 h with gentle stirring. The terminal Au NPs concentration was 0.5 nM. Particles were then separated from unbound serum by centrifugation (14000*g* for 20 min at 4 °C). Protein concentration in supernatant was then determined using a BCA protein assay reagent kit. As a control for nonspecific protein adsorption, equal concentrations of Au NPs without ligands (Au NPs@ LA-NR$^4$+LA-PEG) were treated in parallel (Figure S2, Supporting Information).

**2.11. Cell Uptake and Toxicity.** HepG2 cells were grown in a cell culture flask using DMEM (Solarbio Science & Technology Co., Ltd., Beijing) supplemented with 10% fetal bovine serum at 37 °C in an atmosphere of 5% $CO_2$. For NP uptake studies, cells were seeded 1105 cells/well in 24-well plates and incubated for 1 day to allow for cell attachment. Then cell medium was removed and replaced with 1 mL of 0.8 nM Au NPs in serum containing media and incubated for 3 h. The medium was then discarded and cells were washed three times with PBS. Samples were digested overnight in 1 mL of aqua regia, and diluted in 5 mL of $H_2O$. The gold nanoparticle sample solution was measured by ICP-MS (X7 Series, Thermo Electron Corporation, USA). Cell viability was measured using the MTT assay. HepG2 cells were seeded 8000 cells/well in 96-well plates and incubated for 1 day to allow for cell attachment. The old medium was replaced with 150 mL of freshly prepared medium containing Au NPs at concentrations of 0.5, 1 and 2 nM and incubated for 24 h. Then, MTT solution was added followed by incubation for another 4 h. After washed three times with PBS, 100 $\mu$L of dimethyl sulfoxide (DMSO) was added to each well to dissolve the formazan crystals. The absorbance was measured by a microplate reader at 570 nm. Cells incubated only with media were used as a blank control.

## 3. RESULTS AND DISCUSSION

**3.1. Synthesis of LA-PEG-GA-N(CH$_3$)$_2$ and LA-NR$^n$.** To obtain AuNPs with an ultrasensitive pH-response self-assemble/disassemble ability, we synthesized heterofunctional lipoyl poly(ethylene glycol) with GA-N(CH$_3$)$_2$ (denoted as LA-PEG-GAN(CH$_3$)$_2$) and LA-NR$^n$. First, the GA molecule was modified by attaching a dimethyl amino group to the carboxyl group. This modification imparts GA with pH-dependent hydrophilicity, weakening hydrophobic interactions and promoting the disassembly of Au NPs at lower pH. The synthetic procedure is shown in Scheme 2. Generally, the dimethyl amino group was first attached to the carboxyl group of GA. Then, the hydroxyl group of GA was reacted with succinic anhydride to obtain suc-GA-N(CH$_3$)$_2$ (**3**) with a new carboxyl group, so that it could be immobilized on the terminal of PEG. The amino group on NH$_2$-PEG-OH was first functionalized by reacting with **3**, then the OH group at the other end was reacted with $\alpha$-lipoic acid to give LA-PEG-GA-N(CH$_3$)$_2$. The $^1$H NMR spectra are depicted in Figure 1, where all characteristic peaks of GA-N(CH$_3$)$_2$, PEG and LA can be found. For example, the peaks at 5.70 ppm (−C═CHCO−) and 4.53 ppm (−CH—OCO−) are attributed to the proton of GA. The sharp peak at 3.64 ppm is attributed to the methylene protons of the PEG block (−CH$_2$CH$_2$O−). Further detailed assignments of peaks can be found in Figure 1. The MALDI-TOF MS spectra of **5** are shown in Figure 2. Mainly, $m/z$ signals of **5** were about 811.6 higher than that of the starting NH$_2$-PEG-OH, consistent with the molecular weight calculation (640.5 for **3** + 206.3 for LA-18.0 × 2 for 2 H$_2$O = 810.8).

LA-NR$^n$ derivatives were synthesized readily by amidation reaction in the presence of EDC·HCl. The hydrophobicity of LA-NR$^n$ can be precisely tuned by various hydrophobic substituents. Citric acid-stabilized AuNPs (~26 nm, measured by DLS) were prepared according to the literature. LA-PEG-GA-N(CH$_3$)$_2$ and LA-NR$^n$ were introduced to the citrate gold nanoparticles with surface exchange.

**3.2. Self-Assembly of Au NPs and Their pH Sensitivity.** The assembly of Au NPs (26 nm) modified with LA-N(iPr)$_2$ and LA-PEG-GA(CH$_3$)$_2$ is described here as a representative characterization. The hydrodynamic size of dispersed Au NPs was determined as being 50 nm by dynamic light scattering (DLS) measurements (Figure 3a, blue line). The self-assembly approach of Au NPs is based on a simple high-speed shake (1.5 min) in pH 9.0 aqueous solution, without any assistant materials such as organic solvents, templates or binder molecules. Thus, this simple, green and template-free process shows potential promise for biomedical applications. DLS (Figure 3a, red line) revealed the size of particles increase to 200 nm with a narrow size distribution, which is appropriate for drug delivery and EPR effect in vivo. Formation of the nanostructure assemblies was confirmed by transmission electron microscopy (TEM) imaging. Figure 1b shows a characteristic image of the regular clusters consisting of 10−20 Au nanoparticles for each cluster. The individual cluster size is observed to be 4−5 times larger than single Au NPs, which is consistent with the DLS measurements. The surface plasmon resonance (SPR) band of the assembly solution (Figure 3c) shows an ~10 nm red shift relative to dispersed Au NPs (524 nm), which suggests interparticle plasmonic


dx.doi.org/10.1021/am5045339 | ACS Appl. Mater. Interfaces 2014, 6, 17865−17876

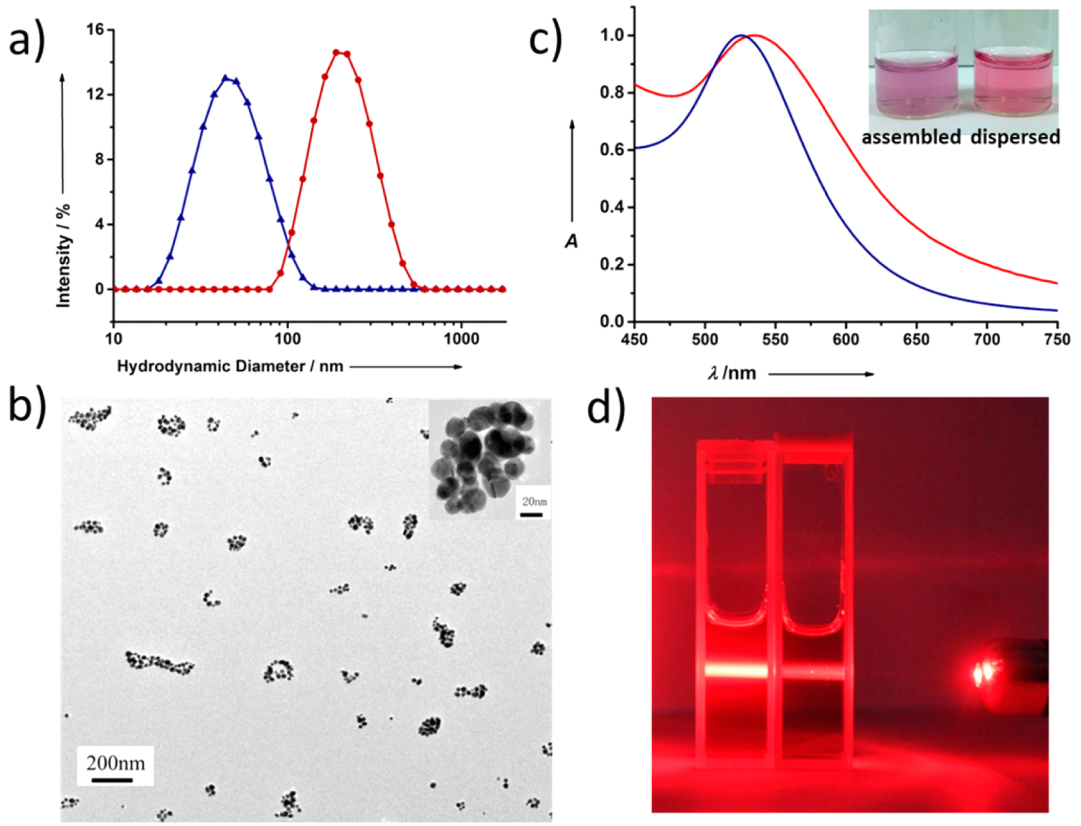


**Figure 3.** Characterization of assembled Au NPs. Au NPs modified with LA-N(iPr)$_2$ and LA-PEG-GA(CH$_3$)$_2$ were used here. (a) Hydrodynamic diameter distribution of dispersed (blue) and assembled (red) gold nanoparticles. (b) TEM image of the assemblies formed by 30 nm gold nanoparticles (dry state diameter). The scale bar for partial enlargement is 20 nm. (c) Absorption spectra and photograph of dispersed AuNPs (blue, peak at 524 nm) and assembled Au NPs (red, peak at 535 nm). The inset photo presents photos for assembled (left) and disassembled (right) Au NPs. (d) Tyndall effect for the assembly (left) and dispersed Au NPs (right) solutions with equal Au concentration.

coupling to some extent. Interestingly, compared to the single Au NPs solution, the Tyndall effect is observed to be much more obvious for an assembled solution with equal concentration (Figure 3d), which confirms the formation of larger particles (based on the Rayleigh equation). It should be noted that TEM images represent the dry state under a high vacuum, and that the nanoparticles hardly retained their spherical morphology without collapsing after they were dried. The aqueous Au NPs assembly, however, showed an insignificant change in the SPR band and size distribution, even after 1 month, suggesting their good stability in solution (Figure S1, Supporting Information).

The formed nanoparticle disassembled rapidly within a subtle pH decrease, and its ultrasensitive pH-response allowed the variation of transition pH values through the precise control of hydrophobic substituents on LA-NR$^n$. A series of lipoyl amines were synthesized (Figure 4a) and grafted onto the surface of Au NPs with LA-PEG-GA-N(CH$_3$)$_2$. Subsequently, the Au NPs were assembled using the method mentioned before. The hydrodynamic sizes of a series of Au NPs in solutions at different pH values (Figure 4b–d) illustrated a sharp volume transition for each assembled nanoparticle. DLS data showed the pH transition points were at 8.0, 7.4 and 7.2 for LA-NR$^2$, LA-NR$^3$ and LA-NR$^4$, respectively, decreasing with the hydrophilicity of substituents on the tertiary amines. The disruption of the assembly was achieved immediately at a point lower than the transition point with the pH 0.2, which indicated that the sharpness values were about 0.2 pH units for each group. The diameter of Au NPs with LA-NR$^1$ is observed to be always 50 nm. In contrast, strong hydrophobicity of dibutyl amino (LA-NR$^5$) inhibits disassembly of NPs, only swelling instead of disrupting, even at pH 6.5 (data are not included here). The shift of the SPR band varying with pH was also used to monitor the disassembly of Au NPs by UV, which coincides with the DLS measurement. Figure 4e shows the variation of the position of the SPR band at different pH values for Au NPs with LA-NR$^4$ and PEG-GA-N(CH$_3$)$_2$, which suggests the interparticle plasmonic coupling became weaker below pH 7.4. These data also illustrate that the hydrophobicity of the dimethyl amino group plays an important role for assembly and disassembly. Most importantly, Au NPs grafting with LA-NR$^4$ having pH 7.2 transition points can ideally respond to normal tissue pH (pH 7.4) and tumor extracellular pH (pHe 6.8), which is expected to be stable in the blood whereas dispersed totally at the tumor site. This unique sensitivity and rapid response is rare for the nanostructure assembled from inorganic nanoparticles. Thus, the system with LA-NR$^4$ was used for the following experiments.

**3.3. Mechanism Study of GA's Shield.** Au NPs act as good quenchers of many fluorescence donors due to the nanosurface energy transfer (NSET) effect,[22] which suggests that the fluorescence quenching happens when fluorophores are entrapped inside assembled structures formed by Au NPs. To validate the pH-response value and elucidate the microenvironment of assembled NPs for the possibility of ligand's shield, the fluorescence spectra (Figure 5a) of NPs loaded with pyrene and obtained at different pH values were measured. Pyrene is selected as a model fluorophore because it is a pH-insensitive fluorescence

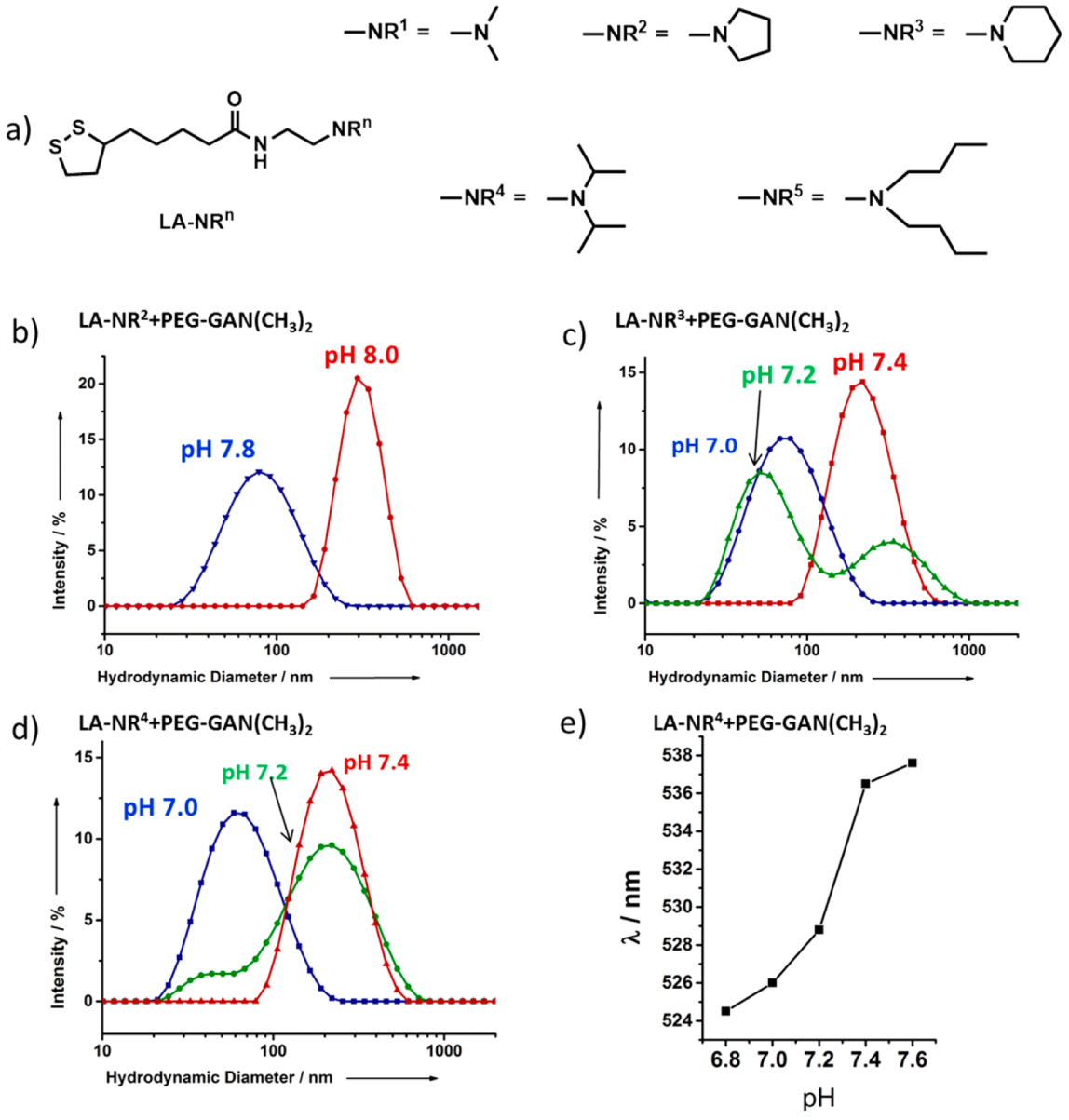


**Figure 4.** (a) Structures of LA-NR$^n$. (b–d) Representative DLS datas of LA-NR$^2$ (b), LA-NR$^3$ (c) and LA-NR$^4$ (d) at different pH values. Assemblies disrupted into single Au NPs within the change of 0.2 pH units, but at different transition pH values. (e) Plot of the variation of the position of the SPR band for Au NPs@LA-NR$^4$+PEG-GA-N$(CH_3)_2$ at various pH values.

probe with high hydrophobicity that can be loaded into assemblies easily by a film-rehydration method. The results revealed that the fluorescence intensity of the same amount of pyrene loaded above pH 7.2 was much weaker than that below pH 7.0, and it showed a significant increase between pH 7.2 and 7.0, with a platform below pH 6.8. The fluorescence emission of pyrene trapped in the hydrophobic core can be absorbed by the gold nanoparticles, which leads to lower fluorescence, whereas the rapid recovery of fluorescence at pH 7.0 suggests the exposure of pyrene from NPs. In addition, an increase in the ratio of the first (373 nm) and third (384 nm) vibronic peak intensities ($I_1/I_3$) from pH 7.6 to 6.8 in the spectrum was observed (Figure 5b). The value of the $I_1/I_3$ emission intensity ratio is very sensitive to the polarity of the medium surrounding pyrene molecules where a larger the ratio corresponds to the bigger polarity of the medium. The increase in $I_1/I_3$, especially the jump between pH 7.2 and 7.0, indicates the increased polarity of microenvironments of pyrene with the decreased pH. Consistent with the data obtained by from DLS measurements, both fluorescence spectra data analysis indicate that the assemblies remain stable above pH 7.2, whereas the immediate disruption of assembly occurs within the decreasing 0.2 pH unit, and the total dispersion of NPs dispersed into single Au NPs happens below pH 7.0. Nile red (NR), another microenvironment-sensitive fluorescent probe, was also applied to examine its pH response.[31] The spectra of NR in Au NPs solution (Figure 5c) below pH 7.0 showed a significant red shift relative to that above pH 7.2 due to the sharp increase of polarity around the probe from pH 7.2 to pH 7.0. It is noticed that the fluorescence intensity of Nile red decreases below pH 7.2, just contrary to that of pyrene. This is because the fluorescence of Nile red is quite weak in aqueous solutions but is known to increase substantially in the hydrophobic environments, which just confirmed the release of Nile red from the assembly below pH 7.2. The data strongly corroborated the super sharp pH sensitivity (~0.2 pH) and the hydrophobic microenvironment inside the assembly, which pointed to the


dx.doi.org/10.1021/am5045339 | ACS Appl. Mater. Interfaces 2014, 6, 17865–17876

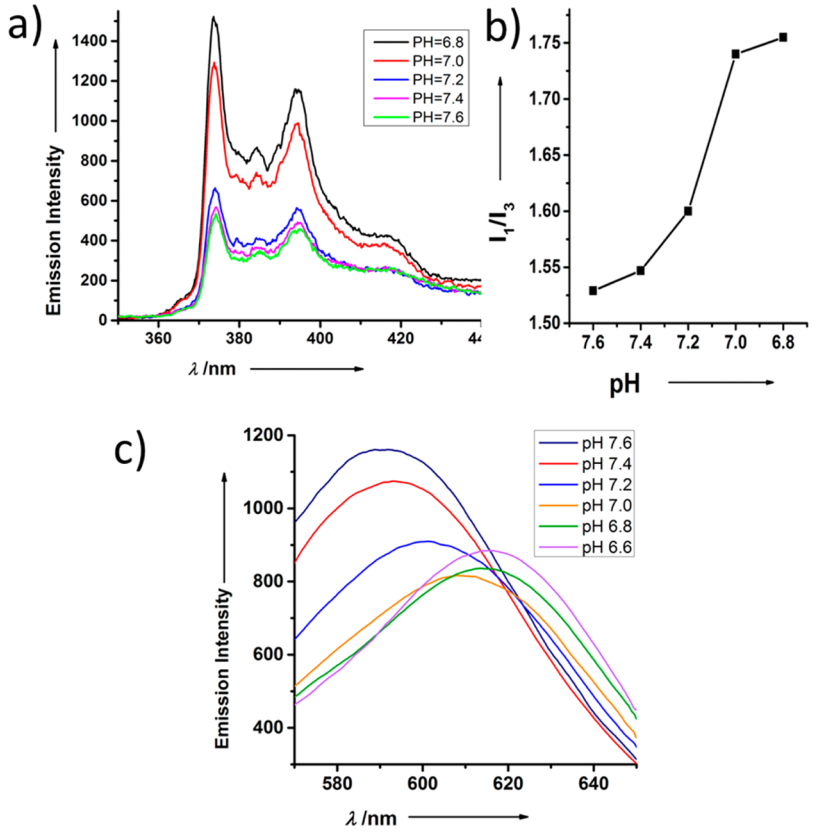


**Figure 5.** (a) Fluorescent intensity of Au NPs assembly loading pyrene at pH 7.6, 7.4, 7.2, 7.0 and 6.8 at the same concentration. (b) Ratio of the first (373 nm) and third (384 nm) peak intensities ($I_1/I_3$) as a function of pH value. (c) Fluorescence spectra of Au NPs assembly loading Nile red at pH 7.6, 7.4, 7.2, 7.0, 6.8 and 6.6.

existence of hydrophobic segments including GA in the assembly's interior at pH 7.4 for ligand shielding.

To study mechanically the possibility for GAs' shield, we compared Au NPs' analogues assembly behavior (Table S1, Supporting Information). Au NPs mediated simply by low molecular tertiary amine molecules would aggregate extensively and irreversibly within a short time, hence the PEG derivative was introduced. But for common PEG, which is a highly hydrophilic polymer, the self-assembly behavior is impeded due to inhibition of the interparticle interactions. Hydrophilicity of PEG was tuned by immobilizing a hydrophobic GA molecule, in order to reach a compromise between interparticle repulsion and over plasmonic coupling of Au NPs. Au NPs with LA-PEG-GA and LA-NR[4] can assemble into nanoparticles spontaneously, but they were stable regardless of the varying pH, probably owing to GA's high hydrophobicity. A dimethyl amino group was attached to the GA molecule for improved hydrophilicity varying with pH, which was demonstrated through investigating the size of nanoparticle formed by mPEG-GA-N$(CH_3)_2$, whose size is pH-dependent. The apparent p$K_a$ of this polymer was found to be around 7.7 (Figure S2, Supporting Information). Figure 6 shows the size of the particles increased with decreasing pH, which suggested the improvement of hydrophilicity from pH 8 to 6. The pH trigger was in a physiological relevant range. This pH dependent hydrophobicity provides not only the driving force to the Au NPs assembly but also reduces the attractive force for the disassembly at lower pH by the protonated amine groups. On the other hand, LA-NR$^n$ also played a significant role in both assembly and disassembly. The $\zeta$-potentials of Au NPs at different pH values were measured (Figure 6c). As expected, the potential of Au NPs becomes more positive with the decrease of pH. It is worthwhile to note that the increment of $\zeta$-potential between pH 7.4 and 6.8 is more obvious than that of Au NPs@LA-NR[4]+PEG (Figure S3, Supporting Information), which may attributed to the burying of amine and GA-N$(CH_3)_2$ when the assembly formed. Of course, any pH-responsive disassembly behavior was not observed in the absence of LA-NR$^n$. Thus, we speculated that two delicate balances drive the formation of the assembly at a higher pH: (1) the pH-dependent ionization equilibrium between the positively charged tertiary ammonium groups and the neutral hydrophobic tertiary amines[32] and (2) the achievement of appropriate assembly force from hydrophobicity in GA and tertiary amine segment after a critical threshold. The PEG block on the shell provided repulsion, impeding further aggregation, which allowed the assembly's thermodynamic stability for a long time. In the case of disassembly of the nanostructures, it was attributed to the superiority of increased electrostatic repulsion of each Au NPs from the protonated amine groups at a lower pH.

Due to the above data analysis that the microenvironment inside the assembly is hydrophobic and GA provides the major hydrophobic force for assembling, we propose GA ligands located into the core of assembly or the microinterstice between Au NPs act as an "adhesive" to conglutinate several gold particles into an assembly. Thus, GA ligands may be hidden when the assembly is formed.

**3.4. BSA Absorption for Assembled and Dispersed Au NPs.** To evaluate whether GA can be shielded by the assembly, we studied the assembly's and disassembly's absorption with bovine serum albumin (BSA) molecules, which has a strong

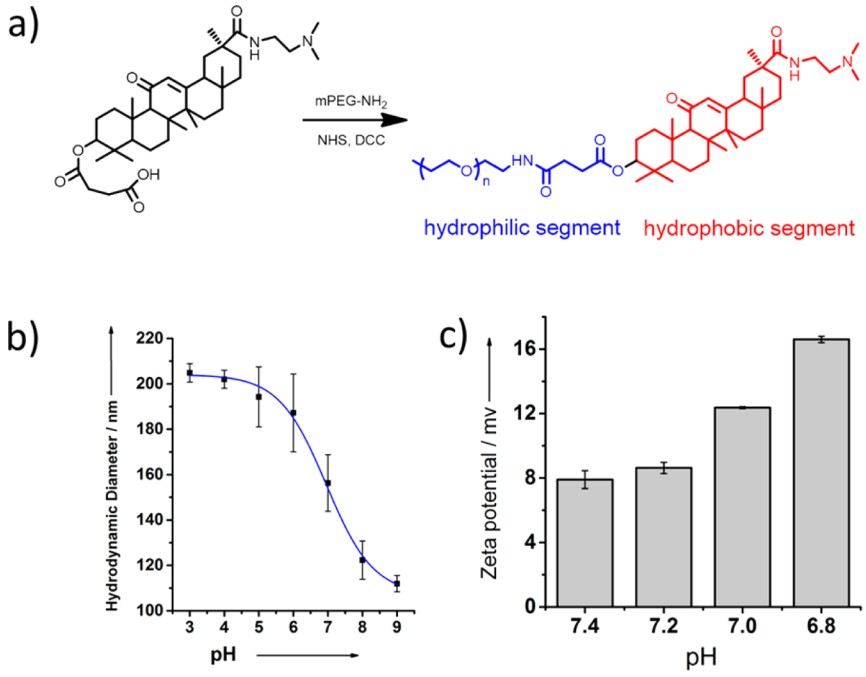


**Figure 6.** (a) Synthesis of mPEG-N$(CH_3)_2$. (b) Size of the particles formed by PEG-GA-N$(CH_3)_2$ increased with decreasing pH. (c) ζ-Potentials of Au NPs at pH 7.4, 7.2, 7.0 and 6.8.

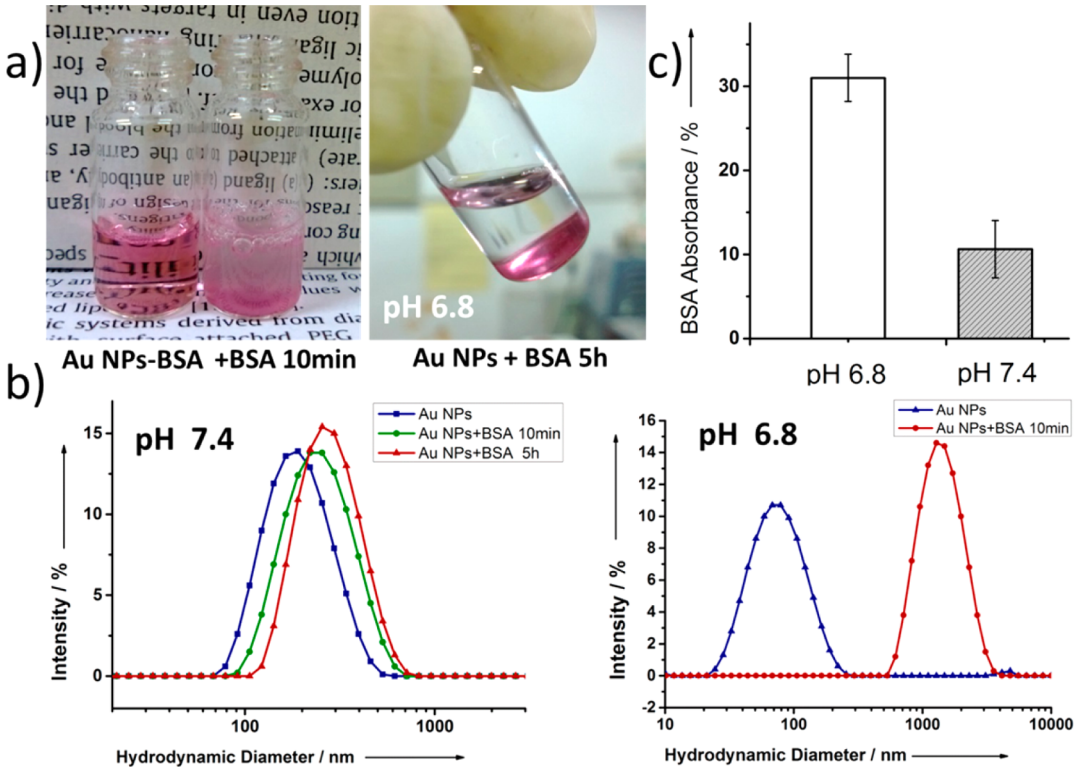


**Figure 7.** (a) Photograph of Au NPs before and after the addition of BSA for 10 min and 5 h at pH 6.8. (b) Hydrodynamic diameters for Au NPs before and after the addition of BSA at pH 6.8 and 7.4. (c) Serum protein adsorptions on Au NPs at pH 6.8 (white bar) and pH 7.4 (gray bar) measured by the bicinchoninic acid (BCA) assay.

binding constant with GA molecules.[33] As shown in Figure 7a, stirring the Au NPs at pH 6.8 with BSA resulted in reduced transparency of the solution significantly after 10 min, and showed a broadening absorption with higher absorbance (Figure S4, Supporting Information), where the agglomerates finally flocculate onto the tube bottom after 5 h. On the contrary, BSA scarcely changed the solution of Au NPs at pH 7.4. The DLS result (Figure 7b) shows the formation of aggregated Au NPs at pH 6.8 with the size of 1000 nm, but assembled Au NPs with BSA at pH 7.4 show almost no spectral change along with any obvious variation in size. This obvious contrast may be attributed to the collision frequency of GA that is exposed on the surface of NPs


dx.doi.org/10.1021/am5045339 | ACS Appl. Mater. Interfaces 2014, 6, 17865−17876

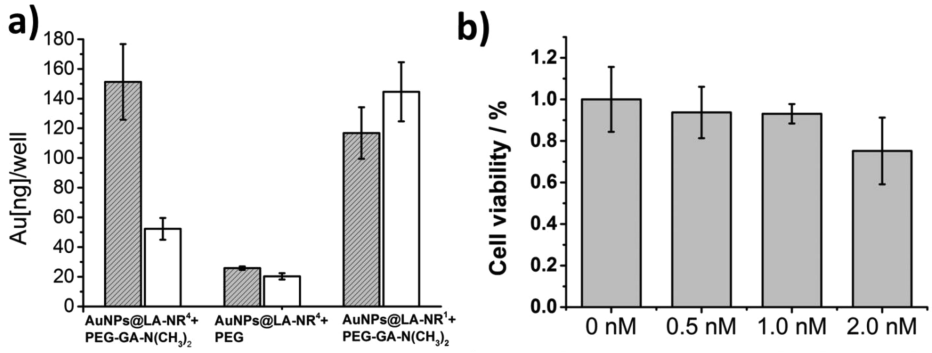


**Figure 8.** (a) Cellular uptake of Au NPs@LA-$NR^4$+PEG-GA-$N(CH_3)_2$, Au NPs@LA-$NR^4$+PEG and Au NPs@LA-$NR^1$+PEG-GA-$N(CH_3)_2$ at pH 6.8 (gray bar) and pH 7.4 (white bar) measured by ICP-MS. (b) Viability of cells exposed to Au NPs with different concentrations (0.5, 1.0, 2.0 nM) for 24 h.

and BSA molecules. The formation of assembled NPs enables the shielding of GA ligands with a decrease of interaction with BSA.

To quantitatively study the effect of assembly on serum protein adsorption, we incubated diluted Au NPs samples in BSA solution (0.5 mg/mL) and measured total protein adsorption by the bicinchoninic assay (BCA) (Figure 7c). For the assembled sample at pH 7.4, about 70% of serum protein adsorption was eliminated relative to dispersed nanoparticles at pH 6.8, confirming the shielding effect. Au NPs grafted with LA-$NR^4$ and LA-$PEG_{2k}$ were used as control samples for which no significant difference was observed between pH 6.8 and 7.4 (Figure S5, Supporting Information). The results indicated that it is mainly the difference of GA exposure instead of the difference of amino protonation at pH 6.8 and 7.4 that induces the different adsorption of the negative charged protein for our simple. The assembly is expected to avoid serum protein adsorption during the blood circulation, thus escaping reticuloendothelial system recognition.

**3.5. In Vitro Cellular Uptake.** Cellular uptakes of Au NPs@PEG-GA-$N(CH_3)_2$ and Au NPs@PEG-GA were conducted to confirm the affinity of the GA derivative (Figure S6 in the Supporting Information). Further evidence of the GA ligand's shield in the state of assembly was provided in Figure 8, where the cellular uptake of the assembled and disassembled Au NPs is quantified using inductively coupled plasma mass spectrometry (ICP-MS). Human hepatocellular carcinoma (HepG2) cells that express the receptor of GA[28] were incubated with Au NPs at pH 6.8 or 7.4. As the ICP-MS analysis shows in Figure 8a, the dispersed Au NPs demonstrate an obvious increase in cellular uptake that is about 3 times the amount of the assembly taken up. As control subjects, cellular uptakes of Au NPs without ligands (Au NPs@LA-$NR^4$+LA-PEG) and Au NPs with LA-$NR^1$ (Au NPs@LA-$NR^1$+LA-PEG-GA-$N(CH_3)_2$) were examined. Due to the absence of GA or LA-$NR^4$ for these two groups, not enough hydrophobic forces were provided for the assembly, both of them remain dispersed regardless of pH changes. ICP-MS analysis revealed that the cellular internalization was nearly identical for Au NPs without GA at pH 6.8 and 7.4, which indicates that amino protonation difference cannot be the major source for different cellular uptakes. For Au NPs with LA-$NR^1$ and GA-$N(CH_3)_2$, the amount taken up by cells at pH 6.8 was even less than that at pH 7.4, which can be attributed to the increase of surface hydrophobicity of Au NPs at pH 7.4 that facilitates cellular uptake. Obvious contrast in cellular uptake between Au NPs with and without GA was observed, but the contrast was much smaller between Au NPs in the assembled state at pH 7.4 and Au NPs without GA. In other words, cellular uptake was amplified significantly for dispersed GA-attached Au NPs. This not only suggests the effects of GA's shield when assembly formed but also indicates the ligand-mediated uptake for our system instead of simple size change of nanoparticles between assembly and disassembly. All these results show the possibility that the assembly can bury the hydrophobic GA ligands inside assembly, thus decreasing interfacial GA density on the corona of the self-assembly. This efficiently inhibits its interaction with receptors on cell membrane at 7.4. The rapid disassembly at tumor extracellular pH endows the recovery of Au NPs' targeting ability, facilitating cellular uptake. MTT assays were performed to assess the cytotoxicity of our sample against HepG2 cells, which showed negligible cytotoxicity even at high Au concentrations (Figure 8b).

**3.6. Reversibility of Au NPs' Assembly.** Reassembly was easier than initial assembly, which can be obtained by gentle shaking at pH 7.4. The assembly/disassembly process was reversible for cycles by switching the pH value between 6.8 and 7.4 by acid−base titration (Figure 9). DLS data indicated that

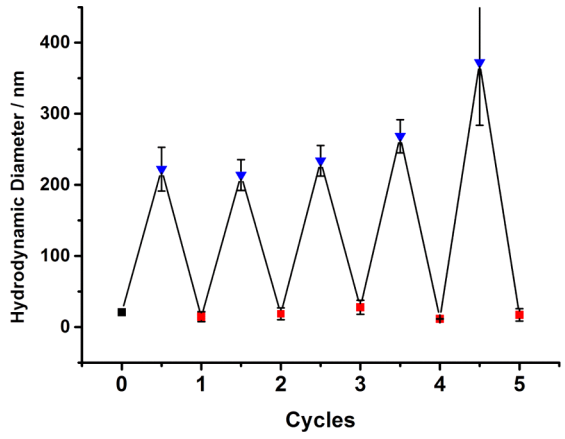


**Figure 9.** Reversible assembly and disassembly of Au NPs as detected by DLS upon the alternation of pH 6.8 and 7.4 (Au NPs of ~10 nm were used here[34]).

the hydrodynamic diameter of assembly remained constant (200−250 nm) with a narrow distribution at pH 7.4 during the cycles, which meant that the dispersed Au NPs could reassemble efficiently into nanoparticles again when the solution was titrated back to basic pH. On the contrary, the immediate decrease of size at pH 6.8 suggests that Au NPs can be well dispersed even after cycles. To the best of our knowledge, it is rare for inorganic nanoparticles to achieve a reversible assembly/disassembly

behavior responding to such extrinsic pH changes in a clinically relevant range.

## 4. CONCLUSIONS

In summary, we developed a new approach for pH-sensitive controllable tumor targeting by the assembly/disassembly of Au NPs. Ordered assembly of Au NPs and ultrasharp pH sensitivity were achieved by the fine-tuning of materials modified on Au NPs. Owing to the unique design that hydrophobic GA ligands provided the major interparticle attractive force, the amphiphilic assembly of Au NPs led to the shield of GA, giving an efficient decrease of BSA absorption and cellular uptake. Due to the excellent pH response of Au NPs' nanostructures, GA could be exposed immediately when disassembled. Moreover, the reversibility of assembly/disassembly strongly implies the potential for reversible shielding and deshielding, which surmounts the irreversibility of traditional shieldable carriers.

## ■ ASSOCIATED CONTENT

### Supporting Information

Hydrodynamic size change of assembly, pH-profile of PEG-GA-$N(CH_3)_2$, UV−vis spectra of AuNPs with BSA, BSA absorptions and $\zeta$-potentials of control groups. This material is available free of charge via the Internet at http://pubs.acs.org.

## ■ AUTHOR INFORMATION

### Corresponding Author

*Z. Yuan. E-mail: zhiy@nankai.edu.cn.

### Notes

The authors declare no competing financial interest.

## ■ ACKNOWLEDGMENTS

This work was supported by National Natural Science Foundation of China (51433004, 51273095), State Key Fundamental R&D Project (2011CB606202), Natural Science Foundation of Tianjin (13JCYBJC25100), and PCSIRT (IRT1257). We also appreciated for the kind support from Prof. Yongmei Wang.

## ■ REFERENCES

(1) Petros, R. A.; DeSimone, J. M. Strategies in the Design of Nanoparticles for Therapeutic Applications. *Nat. Rev. Drug Discovery* **2010**, *9*, 615−627.

(2) Farokhzad, O. C.; Langer, R. Impact of Nanotechnology on Drug Delivery. *ACS Nano* **2009**, *3*, 16−20.

(3) Tonga, G. Y.; Saha, K.; Rotello, V. M. 25th Anniversary Article: Interfacing Nanoparticles and Biology: New Strategies for Biomedicine. *Adv. Mater.* **2014**, *26*, 359−370.

(4) Deng, C.; Jiang, Y.; Cheng, R.; Meng, F.; Zhong, Z. Biodegradable Polymeric Micelles for Targeted and Controlled Anticancer Drug Delivery: Promises, Progress and Prospects. *Nano Today* **2012**, *7*, 467−480.

(5) Yoo, J. W.; Doshi, N.; Mitragotri, S. Adaptive Micro and Nanoparticles: Temporal Control over Carrier Properties to Facilitate Drug Delivery. *Adv. Drug Delivery Rev.* **2011**, *63*, 1247−1256.

(6) Yan, Y.; Such, G. K.; Johnston, A. P. R.; Best, J. P.; Caruso, F. Engineering Particles for Therapeutic Delivery: Prospects and Challenges. *ACS Nano* **2012**, *6*, 3663−3669.

(7) Mura, S.; Nicolas, J.; Couvreur, P. Stimuli-Responsive Nanocarriers for Drug Delivery. *Nat. Mater.* **2013**, *12*, 991−1003.

(8) Sun, Q.; Radosz, M.; Shen, Y. Challenges in Design of Translational Nanocarriers. *J. Controlled Release* **2012**, *164*, 156−169.

(9) Lee, E. S.; Na, K.; Bae, Y. H. Super pH-Sensitive Multifunctional Polymeric Micelle. *Nano Lett.* **2005**, *5*, 325−329.

(10) Du, J. Z.; Sun, T. M.; Song, W. J.; Wu, J.; Wang, J. A Tumor-Acidity-Activated Charge-Conversional Nanogel as an Intelligent Vehicle for Promoted Tumoral-Cell Uptake and Drug Delivery. *Angew. Chem., Int. Ed.* **2010**, *49*, 3621−3626.

(11) Fan, N.-C.; Cheng, F.-Y.; Ho, J.-a. A.; Yeh, C.-S. Photocontrolled Targeted Drug Delivery: Photocaged Biologically Active Folic Acid as a Light-Responsive Tumor-Targeting Molecule. *Angew. Chem.* **2012**, *124*, 8936−8940.

(12) Song, N.; Ding, M.; Pan, Z.; Li, J.; Zhou, L.; Tan, H.; Fu, Q. Construction of Targeting-Clickable and Tumor-Cleavable Polyurethane Nanomicelles for Multifunctional Intracellular Drug Delivery. *Biomacromolecules* **2013**, *14*, 4407−4419.

(13) Jin, E.; Zhang, B.; Sun, X.; Zhou, Z.; Ma, X.; Sun, Q.; Tang, J.; Shen, Y.; Van Kirk, E.; Murdoch, W. J.; Radosz, M. Acid-Active Cell-Penetrating Peptides for in Vivo Tumor-Targeted Drug Delivery. *J. Am. Chem. Soc.* **2013**, *135*, 933−940.

(14) Zhang, J.; Yuan, Z. F.; Wang, Y.; Chen, W. H.; Luo, G. F.; Cheng, S. X.; Zhuo, R. X.; Zhang, X. Z. Multifunctional Envelope-Type Mesoporous Silica Nanoparticles for Tumor-Triggered Targeting Drug Delivery. *J. Am. Chem. Soc.* **2013**, *135*, 5068−5073.

(15) Wang, S.; Wang, H.; Liu, Z.; Wang, L.; Wang, X.; Su, L.; Chang, J. Smart pH- and Reduction-Dual-Responsive Folate-PEG-Coated Polymeric Lipid Vesicles for Tumor-Triggered Targeted Drug Delivery. *Nanoscale* **2014**, *6*, 7635−7642.

(16) Chen, Y.; Ai, K.; Liu, Y.; Lu, L. Tailor-Made Charge-Conversional Nanocomposite for pH-Responsive Drug Delivery and Cell Imaging. *ACS Appl. Mater. Interfaces* **2013**, *6*, 655−663.

(17) Macewan, S. R.; Chilkoti, A. Controlled Apoptosis by a Thermally Toggled Nanoscale Amplifier of Cellular Uptake. *Nano Lett.* **2014**, *14*, 2058−2064.

(18) Macewan, S. R.; Chilkoti, A. Digital Switching of Local Arginine Density in a Genetically Encoded Self-Assembled Polypeptide Nanoparticle Controls Cellular Uptake. *Nano Lett.* **2012**, *12*, 3322−3328.

(19) Yao, X.; Peng, R.; Ding, J. Cell−Material Interactions Revealed Via Material Techniques of Surface Patterning. *Adv. Mater.* **2013**, *25*, 5257−5286.

(20) Ling, D.; Park, W.; Park, S. J.; Lu, Y.; Kim, K. S.; Hackett, M. J.; Kim, B. H.; Yim, H.; Jeon, Y. S.; Na, K.; Hyeon, T. Multifunctional Tumor pH-Sensitive Self-Assembled Nanoparticles for Bimodal Imaging and Treatment of Resistant Heterogeneous Tumors. *J. Am. Chem. Soc.* **2014**, *136*, 5647−5655.

(21) Chauhan, V. P.; Jain, R. K. Strategies for Advancing Cancer Nanomedicine. *Nat. Mater.* **2013**, *12*, 958−962.

(22) Song, J.; Zhou, J.; Duan, H. Self-assembled Plasmonic Vesicles of SERS-Encoded Amphiphilic Gold Nanoparticles for Cancer Cell Targeting and Traceable Intracellular Drug Delivery. *J. Am. Chem. Soc.* **2012**, *134*, 13458−13469.

(23) Durand-Gasselin, C. l.; Capelot, M.; Sanson, N.; Lequeux, N. Tunable and Reversible Aggregation of Poly(ethylene oxide-st-propylene oxide) Grafted Gold Nanoparticles. *Langmuir* **2010**, *26*, 12321−12329.

(24) Nikolic, M. S.; Olsson, C.; Salcher, A.; Kornowski, A.; Rank, A.; Schubert, R.; Fromsdorf, A.; Weller, H.; Forster, S. Micelle and Vesicle Formation of Amphiphilic Nanoparticles. *Angew. Chem., Int. Ed.* **2009**, *48*, 2752−2754.

(25) Kairdolf, B. A.; Nie, S. Multidentate-Protected Colloidal Gold Nanocrystals: pH Control of Cooperative Precipitation and Surface Layer Shedding. *J. Am. Chem. Soc.* **2011**, *133*, 7268−7271.

(26) Niikura, K.; Iyo, N.; Matsuo, Y.; Mitomo, H.; Ijiro, K. Sub-100 nm Gold Nanoparticle Vesicles as a Drug Delivery Carrier enabling Rapid Drug Release upon Light Irradiation. *ACS Appl. Mater. Interfaces* **2013**, *5*, 3900−3907.

(27) Zhang, C.; Wang, W.; Liu, T.; Wu, Y.; Guo, H.; Wang, P.; Tian, Q.; Wang, Y.; Yuan, Z. Doxorubicin-Loaded Glycyrrhetinic Acid-Modified Alginate Nanoparticles for Liver Tumor Chemotherapy. *Biomaterials* **2012**, *33*, 2187−2196.

(28) Tian, Q.; Zhang, C. N.; Wang, X. H.; Wang, W.; Huang, W.; Cha, R. T.; Wang, C. H.; Yuan, Z.; Liu, M.; Wan, H. Y.; Tang, H. Glycyrrhetinic Acid-Modified Chitosan/Poly(ethylene glycol) Nano-

particles for Liver-Targeted Delivery. *Biomaterials* **2010**, *31*, 4748−4756.
(29) Frens, G. Controlled Nucleation for the Regulation of the Particle Size in Monodisperse Gold Suspensions. *Nature (London), Phys. Sci.* **1973**, *241*, 20−22.
(30) Beseda, I.; Czollner, L.; Shah, P. S.; Khunt, R.; Gaware, R.; Kosma, P.; Stanetty, C.; Del Ruiz-Ruiz, M. C.; Amer, H.; Mereiter, K.; Da Cunha, T.; Odermatt, A.; Classen-Houben, D.; Jordis, U. Synthesis of Glycyrrhetinic Acid Derivatives for the Treatment of Metabolic Diseases. *Bioorg. Med. Chem.* **2010**, *18*, 433−454.
(31) Levitsky, I.; Krivoshlykov, S. G.; Grate, J. W. Rational Design of a Nile Red/Polymer Composite Film for Fluorescence Sensing of Organophosphonate Vapors Using Hydrogen Bond Acidic Polymers. *Anal. Chem.* **2001**, *73*, 3441−3448.
(32) Zhou, K.; Liu, H.; Zhang, S.; Huang, X.; Wang, Y.; Huang, G.; Sumer, B. D.; Gao, J. Multicolored pH-Tunable and Activatable Fluorescence Nanoplatform Responsive to Physiologic pH Stimuli. *J. Am. Chem. Soc.* **2012**, *134*, 7803−7811.
(33) Zhou, N.; Liang, Y. Z.; Wang, B.; Wang, P.; Chen, X.; Zeng, M. M. Interaction of Glycyrrhetinic Acid, Furosemide and Hydrochlorothiazide with Bovine Serum Albumin and Their Displacement Interactions: Capillary Electrophoresis and Fluorescence Quenching Study. *Biomed. Chromatogr.* **2008**, *22*, 223−231.
(34) Jana, N. R.; Gearheart, L.; Murphy, C. J. Seeding Growth for Size Control of 5−40 nm Diameter Gold Nanoparticles. *Langmuir* **2001**, *17*, 6782−6786.